Journal of Engineering Physics and Thermophysics, Vol. 83, No. 1, 2010

A METHOD FOR MEASURING THE SPECIFIC HEAT CAPACITY OF LAYERED STRUCTURES USING THE BOUBAKER POLYNOMIALS EXPANSION SCHEME

K. Boubaker

UDC 536.2.083

An original method is used to measure the specific heat capacity of some layered structures. The conjoint theoretical–experimental measurement protocol is based on photothermal data and polynomial expansion mathematical analysis. The obtained value of the specific heat capacity for a solar cell buffer material is compared to recently reported results.

Keywords: *Specific heat capacity, $ZnIn_2S_4$, condensed matter, photothermal techniques.*

Introduction. In the last few decades, photothermal techniques have become powerful tools for the thermophysical characterization and nondestructive testing (NDT) of various materials [1–6]. These techniques, which involve photoacoustics, photothermal radiometry, and photothermal deflection, focused mainly on measurement of the thermophysical properties of massive or liquid homogeneous materials. In some recent studies, it was noticed that direct measurement of the specific heat capacity of some layered structures was very difficult. In this context, one can cite, among others, the works of L. P. Filippov [7], who proposed some methods employing easily obtainable empirical data for calculation of the heat capacity of liquids, the investigations of E. S. Platunov [8] on automated devices for measuring the thermophysical properties of massive materials and components in the temperature range 100–700 K, and the studies of J. Koreck et al. [9] and Y. D. Huang et al. [10] on the properties of adhesive layers and metal matrix composites [11–15].

In this study, we propose to extend the existing photothermal technique [16–30] to allow measurements of the heat capacity of microlayered $ZnIn_2S_4$ films. In investigations, the Boubaker polynomials expansion scheme is applied to experimental and graphical data.

NDT Photothermal Deflection Protocol. *Experimental Setup.* The photothermal deflection techniques are based on a thermal response to an exogenous heat supply. In fact, when a targeted material receives an amount of heat from a distant source, it acts afterwards as a local source. A detecting device records the consequent thermal response in the ambient fluid or at the material surface.

If the source generates a single-pulse heat flux, the technique is called an indicial response technique (Fig. 1a). In this case, a memory-dotted device is used to analyze the output signal, whose amplitude and duration depend on the material properties. The most used [16–28] is a frequencial response technique (Fig. 1b), where the source provides a modulated energy whiff toward the material with a preset frequency f.

In our setup [24, 25], the heat source (see Fig. 1b) is a common photoelectrical laser diode (with power P = 0.1 W, wavelength $\lambda = 6.7 \cdot 10^{-7}$ m) coupled to a flexible optic fiber. The use of the optic fiber permits independent spatial installation of the heat source and the sample sides. The source modulation is carried out by a mechanical chopper. The transmitted heat is chopped at a preset frequency f (between 2 and 500 Hz). The main part of the mechanical modulator is a pierced wheel located between the free extremity of the optic fiber and the targeted sample surface [8–10]. The wheel speed is controlled by an accurate feedback D.C. motor. The radius of the beam emitted by the photoelectrical laser diode is controlled by an optical micrometrical diaphragm mounted on the mentioned free extremity.

The probe beam crosses the source-excited beam perpendicularly at prefixed height z_0 (also called offset) from the targeted surface. At its path end, the probe beam is focused at a sensor. The sensor-monitored signal is detected and displayed as an analogical output, namely photothermal signal deflection.

ESSTT/Laboratoire de Physique de la Matière Condensée UPDS, Faculté des Sciences de Tunis, 5100 Mahdia, Tunisia; email: mmbb11112000@yahoo.fr. Published in Inzhenerno-Fizicheskii Zhurnal, Vol. 83, No. 1, pp. 74–79, January–February, 2010. Original article submitted July 24, 2008; revision submitted December 22, 2008.

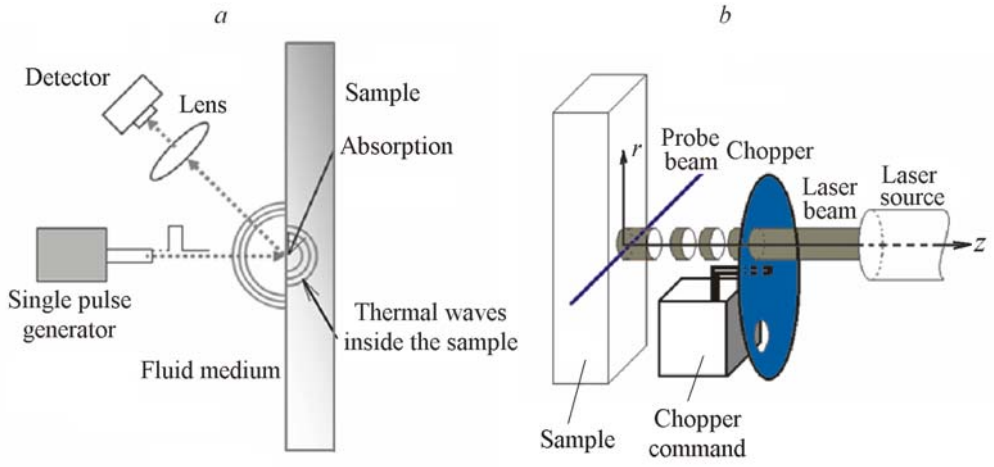

Fig. 1. NDT photothermal deflection techniques: a) indicial response setup; b) frequencial response setup.

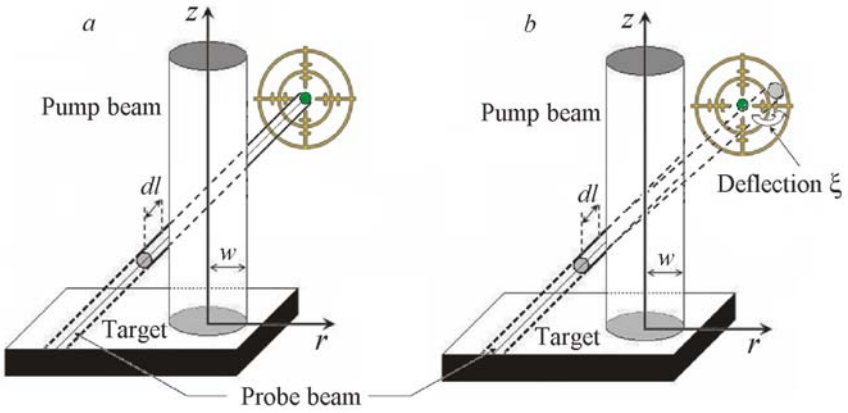

Fig. 2. The probe beam deflection: a) initial path; b) deflected path.

Measurement Technique. The photothermal deflection measurements are based on a thermal response to the modulated heat supply. A detecting device records the consequent thermal response as the deflection of a probe beam that crosses the ambient fluid at the material surface.

The probe beam is provided by a weak laser diode ($P = 10^{-3}$ W, $\lambda = 6.33 \cdot 10^{-7}$ m). The beam path is smoothed by interposing two convergent lens appropriately distanced from the source targeted area. The probe beam offset is fixed at the beginning of each experimental sequence thanks to two endless micrometrical screws bolted to the sample-sink sliding platform [2, 3, 10]. The probe beam path crosses the pump beam perpendicularly (Fig. 1b), then it hits the photodiode cell coupled to a synchronous detection unit.

As the mechanical chopper rates the energy flow to the targeted surface, the photothermal deflection occurs simultaneously and at the same frequency f. Nevertheless, noise and uncontrolled harmonics can interfere with the signal and induce an error. The synchronous deflection detector enables one to avoid the recording of such perturbations, since it is adjusted to detect exclusively the signal with the same chopper frequency, so that variations can be securely attributed to the source effect. An internal synchronous trigger connected to the central unit eliminates any harmonic component with a frequency outside the narrow band centered at the chopper frequency. The synchronous detection unit is composed of an EG&G5210 detector coupled to a plugged-in RS232 interface that transmits the selected and debugged signal to the central unit.

Theory. *Photothermal signal deflection (PSD) components.* In the case of a Gaussian source, the PSD has two components (see Fig. 2): normal and transverse (radial). The expression for the normal component of the probe beam deflection ξ_z is given by the relation [16–18, 32]

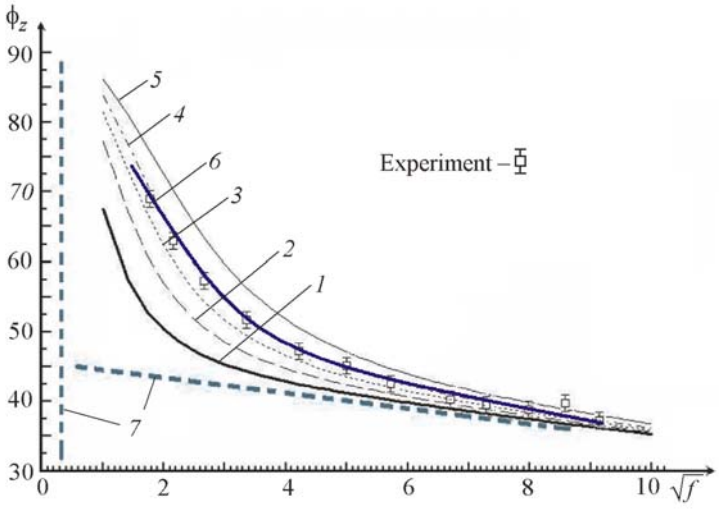

Fig. 3. PSD phase versus $\sqrt{f}$: theoretical curves for different values of D_s ($D_s \cdot 10^5$ = 1 $m^2 \cdot sec^{-1}$ (1); 2 (2); 3 (3); 4 (4); 5 (5)) as well as BPES fitting (6) and asymptotic limits (7). ϕ_z, deg; f, Hz.

$$\xi_z = \frac{1}{T_0} \int_0^\infty \frac{\delta T}{\delta z} dl \,, \tag{1}$$

where dl is the geometrical element of the beam path. In the case of the targeted layers, the theoretical calculation of the normal probe beam deflection ξ_z for a small offset z_0 yields [16–18, 24, 25]

$$\xi_z = \frac{Q_0}{T_0 \alpha w k_s} \sqrt{w^2 + \lambda_s^2} \exp\left(-\frac{z_0}{\lambda_{fl}}\right) \exp(-j\omega t) = |\xi_z| \exp(-j\omega t + \phi_z) \,, \tag{2}$$

where $\lambda_{fl} = \left(\frac{\sqrt{2}}{2} + \frac{\sqrt{2}}{2} j\right) \sqrt{\frac{D_{fl}}{\pi f}}$, $\lambda_s = \left(\frac{\sqrt{2}}{2} + \frac{\sqrt{2}}{2} j\right) \sqrt{\frac{D_s}{\pi f}}$.

Here

$$\phi_z = 45 + \frac{90}{\pi} \arctan \frac{D_s}{\pi f w^2} - \frac{180}{\pi} z_0 \sqrt{\frac{\pi f}{2 D_{fl}}} \,, \tag{3}$$

$$|\xi_z| = \frac{Q_0}{T_0 \alpha w k_s} \left(w^4 + \frac{D_s^2}{\pi^2 f^2}\right) \exp\left(-\frac{\sqrt{2}}{2} z_0 \sqrt{\frac{\pi f}{D_{fl}}}\right). \tag{4}$$

Conjoint Theoretical-Experimental Measurements Protocol. The protocol is based on a set of theoretical curves that give variations of ϕ_z versus the frequency square root $\sqrt{f}$ (Fig. 3) for different values of the thermal diffusivity D_s according to Eq. (3). In the same figure the experimental values ϕ_{zexp} are shown. Furthermore, the experimental fitted dependence ϕ_{zexp} versus $\sqrt{f}$ is obtained by using the Boubaker polynomials expansion scheme (BPES) [26–30]. For this purpose, calculations were carried out by starting from a set of m measured couples $(\phi_{z_i}, \sqrt{f_i})$ with $\sqrt{f_i} \in [\sqrt{f_{i_{min}}}; \sqrt{f_{i_{max}}}]$, where $i = 1, ..., m$,

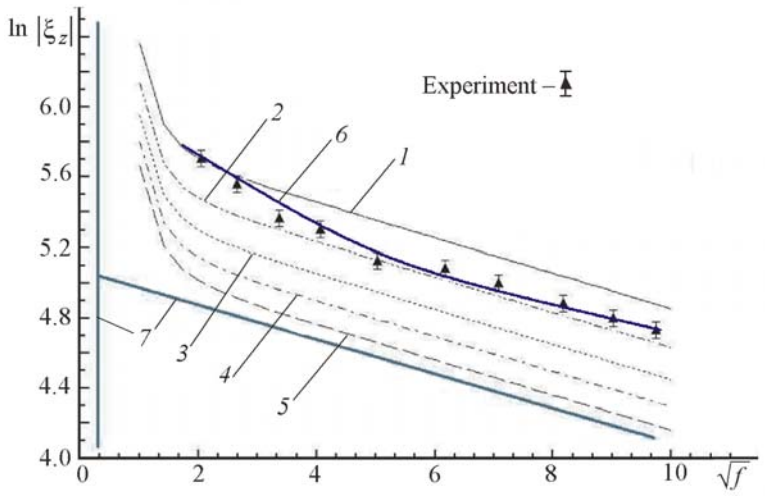

Fig. 4. PSD amplitude versus $\sqrt{f}$: theoretical curves for $D_s = 35.2 \cdot 10^{-6}$ $m^2 \cdot sec^{-1}$ and different values of k_s(k_s = 5 $W \cdot m^{-1} \cdot K^{-1}$ (1); 10 (2); 20 (3); 30 (4); 40 (5)) as well as BPES fitting (6) and asymptotic limits (7). f, Hz.

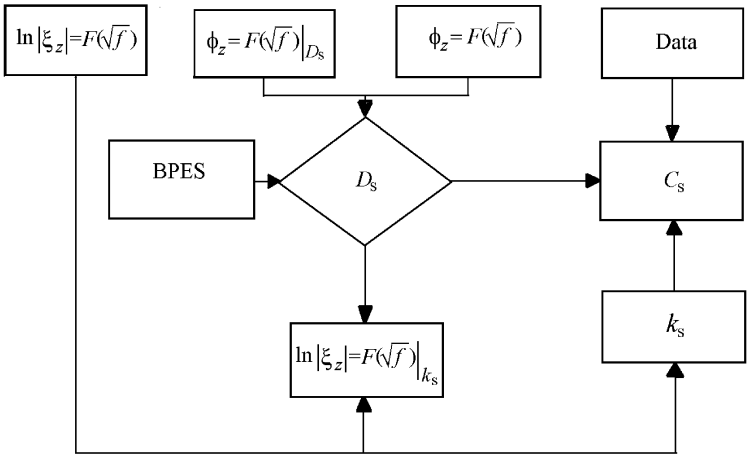

Fig. 5. Theory-experiment conjoint protocol.

$$\phi_{z\exp} = \lim_{N\to\infty}\left[\frac{1}{2N}\sum_{q=1}^{N}\theta_q B_{4q}\left(\frac{\sqrt{f}-\sqrt{f_{i_{\min}}}}{\sqrt{f_{i_{\max}}}-\sqrt{f_{i_{\min}}}}\right)\right]. \tag{5}$$

Here, N is a prefixed integer, B_{4q} (q = 1, 2, ..., N) are $4q$-order Boubaker polynomials, and θ_q are coefficients that minimize the real function F_m

$$F_m = \sqrt{\sum_{i=1}^{m}\left\{\phi_{z_i} - \lim_{N\to\infty}\left[\frac{1}{2N}\sum_{q=1}^{N}\theta_q B_{4q}\left(\frac{\sqrt{f_i}-\sqrt{f_{i_{\min}}}}{\sqrt{f_{i_{\max}}}-\sqrt{f_{i_{\min}}}}\right)\right]\right\}^2}. \tag{6}$$

Equation (5) involving the calculated coefficients θ_q gives the approximate BPES fitting, which is also shown in Fig. 3.

Finally, the approximated value of the thermal diffusivity $D_{s,exp}$ is obtained by applying the Khi2 test to the fitted experimental set of points and choosing the nearest theoretical curve. We obtain $D_{s,exp} = (35.2 \pm 4.5) \cdot 10^{-6}$ $m^2 \cdot sec^{-1}$. The main uncertainties in the obtained value are attributed to the errors introduced by the Khi2 test and the frequency measurement accuracy.

According to expression (4), the PSD amplitude depends on both D_s and k_s. Figure 4 gives the theoretical variation of $\ln|\xi_z|$ versus $\sqrt{f}$ for $D_s = D_{s,exp}$ and different values of the thermal conductivity k_s according to Eq. (4). The same graph shows the experimental values of $\ln|\xi_z|$ and those subjected to the Boubaker polynomials expansion scheme. The approximated value of the thermal conductivity $k_{s,exp}$ is also obtained by considering the theoretical curve nearest to the experimental points. We obtain $k_s = (8.8 \pm 0.9)$ W·m^{-1}·K^{-1}. In Figs. 3 and 4, the asymptotic behavior ($f \to \infty, f \to 0$) of the theoretical dependences is also presented (see lines 7 in the figures mentioned). Finally, the specific heat capacity C_s is deduced [27–29] using the relation

$$C_s = \frac{1}{\rho_s} \frac{k_{s,exp}}{D_{s,exp}} . \quad (7)$$

The obtained value is $C_s = (651.7 \pm 98.0)$ J·K^{-1}·kg^{-1}. The protocol described is summarized in Fig. 5.

Analysis and Conclusions. In the paper, we analyzed theoretical results and numerical data in order to calculate the specific heat capacity of Zn-doped thioindate films. It was noticed [11–18] that the measurement of the thermal characteristics for such materials was a hard task due to low dimensioning and surface roughness effects. We developed a new nondestructive protocol based on photothermal measurements and graphical interpretation. The targeted material has been chosen on the basis of previous studies [31, 32] as a low heat-conductive sample. The results agree very well with the values for similar materials reported in the literature. In fact, the specific heat capacity $C_s \approx 650$ J·K^{-1}·kg^{-1} is not far from the value reported by M. De Otfried [33] and about 14% lower than that presented by S. Picard et al. [34] and S. M. Stishov [35] for similar material at room temperature.

One of the advantages of our method, when compared to the works of M. V. Arx et al. [36], S. Dilhaire et al. [37], and K. Morimoto et al. [38, 39], is that neither special confined measurement apparatus as in [38] nor vacuum chambers as in [39] were needed. Nevertheless, it was experimentally noticed that the validity of the results was limited by the layer thickness of 5 μm.

NOTATION

B_{4q}, $4q$-order Boubaker polynomials; C_s, specific heat capacity, J·K^{-1}·kg^{-1}; D_{fl}, fluid medium thermal diffusivity, m^2·sec^{-1}; D_s, deposited layer thermal diffusivity, m^2·sec^{-1}; f, modulation frequency, Hz; F_m, real function; j, imaginary unit; k_s, deposited layer thermal conductivity, W·m^{-1}·K^{-1}; N, integer; Q_0, deposited heat per unit surface, W·m^{-2}; r, radial coordinate, m; T, absolute temperature, K; T_0, maximum absolute temperature, K; w, Gaussian beam radius, m; z_0, probe beam offset above targeted surface, m; z, axial coordinate, m; α, absorption coefficient, m^{-1}; θ_q, real coefficients in (5) and (6); λ, wavelength, m; ξ, photothermal signal deflection (PSD); $|\xi_z|$, PSD amplitude; ϕ_z, PSD phase, ^{o}; ω, cyclic frequency, Hz. Subscripts: exp, experiment; fl, fluid; max, maximum; min, minimum; s, solid; th, theoretical.

REFERENCES

1. V. P. Kozlov, N. A. Abdel'razak, and N. I. Yurchuk, Physicomathematical models for theories of nondestructive testing of thermophysical properties, *J. Eng. Phys. Thermophys.*, **68**, No. 6, 818–827 (1995).
2. N. P. Zhukov and N. F. Mainikova, Modeling of the process of heat transfer from a plane heat source of constant strength in thermophysical measurements, *J. Eng. Phys. Thermophys.*, **78**, No. 6, 1104–1112 (2005).
3. N. P. Zhukov, Method of nondestructive determination of thermophysical properties of solid materials, *J. Eng. Phys. Thermophys.*, **77**, No. 5, 818–827 (1995).
4. F. Inanc, A backscatter radiography simulation study, *J. Nondestruct. Eval.*, **26**, Nos. 2–4, 33–46 (2007).
5. N. Rajic, An investigation of the bias caused by surface coatings on material loss evaluation by quantitative thermography, *J. Nondestructive Evaluation*, **19**, No. 4, 141–147 (2000).
6. S. Benzerrouk and R. Ludwig, Infrared detection of defects in powder-metallic compacts, *J. Nondestruct. Eval.*, **26**, No. 1, 1–9 (2007).

7. L. P. Filippov, A method for calculating heat capacity and thermal conductivity of liquids, *J. Eng. Phys. Thermophys*., **32**, No. 4, 378–381 (1977).
8. E. S. Platunov, Methods for measurement of thermal conductivity and specific heat at moderate, low, and cryogenic temperatures, *J. Eng. Phys. Thermophys*., **53**, No. 6, 1452–1457 (1987).
9. J. Koreck, C. Valle, J. Qu, and L. J. Jacobs, Computational characterization of adhesive layer properties using guided waves in bonded plates, *J. Nondestruct. Eval.*, **26**, No. 2–4, 97–105 (2007).
10. Y. D. Huang, L. Froyen, and M. Wevers, Quality control and nondestructive tests in metal matrix composites, *J. Nondestruct. Eval.*, **20**, No. 3, 113–132 (2001).
11. Q. Lu, G. Shan, Y. Bai, and L. An, Synthesis and characterization of CdSe/ZnO core/shell nanocrystals, *Int. J. Nanosci.*, **5**, No. 2/3, 299–306 (2006).
12. N. Tabet, M. Faiz, and A. Al-Oteibi, Growth of ZnO nanostructures on zinc and Pt substrates, *Int. J. Nanosci.*, **6**, No. 1, 23–30 (2007).
13. I. P. Kazakov, V. I. Kozlovsky, V. P. Marovitsky, Y. K. Skasyrsky, M. D. Tiberi, A. O. Zabezhaylov, and E. M. Dianov, MBE grown ZnSSe/ZnMgSSe MQW structure for blue VCSEL, *Int. J. Nanosci.*, **6**, No. 5, 407–410 (2007).
14. J. Li, Y. Xu, D. Wu, and Y. Sun, In situ assembly of ZnS nanofibers with highly ordered lamellar microstructure, *Int. J. Nanosci.*, **5**, No. 2/3, 245–251 (2006).
15. X. Bai, E. G. Wang, and Z. L. Wang, Nanomechanics of individual zinc oxide nanobelts measured by in situ transmission electron microscopy, *Int. J. Nanosci.*, **5**, No. 6, 951–958 (2006).
16. F. Saadallah, N. Yacoubi, and A. Hafaiedh, Determination of the thermal properties of semiconductors using the photothermal method in the many thin layers case, *J. Opt. Mater.*, **6**, 35–39 (1996).
17. N. Yacoubi, A. Hafaiedh, and A. Jouille, Determination of the optical and thermal properties of semiconductors using photothermal method, *J. Appl. Opt.*, **33**, No. 30, 7171–7174 (1994).
18. N. Yacoubi, B. Girault, and Jean Fesquet, Determination of absorption coefficients and thermal conductivity of GaAlAs/GaAs heterostructure using a photothermal method, *Appl. Opt.*, **25**, No. 26, 4622–4625 (1999).
19. R. Tilgner and J. Baumann, Photothermal examination of an adhesive layer, *J. Nondestruct. Eval.*, **3**, No. 2, 111–113 (1982).
20. I. Kaufman, P. Chang, H. Hsu, W. Huang, and D. Shyong, Photothermal radiometric detection and imaging of surface cracks, *J. Nondestruct. Eval.*, **6**, No. 2, 87–100 (1987).
21. C. Tai and J. C. Moulder, Bolt-hole corner crack inspection using the photoinductive imaging method, *J. Nondestruct. Eval.*, **19**, No. 3, 81–93 (2000).
22. V. E. Zhuravlev, A. I. Morozov, and V. Yu. Raevskii, Photothermal determination of the thermophysical characteristics of solid-state objects, *J. Eng. Phys. Thermophys*., **56**, No. 1, 79–83 (1989).
23. A. S. Podol'tsev and G. I. Zheltov, Heating of intraocular media by near IR laser radiation, *J. Eng. Phys. Thermophys*., **75**, No. 4, 964–969 (2002).
24. K. Boubaker, M. Bouhafs, and N. Yacoubi, A quantitative alternative to the Vickers hardness test, *J. Nondestruct. Test. Eval.*, **36**, No. 8, 547–551 (2003).
25. K. Boubaker, A new protocol for characterization of dislocations in photovoltaic polycrystalline silicon solar cells, *Sol. Energy Mater. Solar Cells*, **91**, No. 14, 1319–1325 (2007).
26. Ting Gang Zhao, Y. X. Wang, and K. B. Ben Mahmoud, *Int. J. Math. Comput.,* **1**, 13–16 (2008).
27. K. Boubaker, Metal lattice atomic structure characterization using mirage effect technique, *J. Phys. Met. Metallogr.*, **101**, 51–57 (2006).
28. S. Slama, J. Bessrour, K. Boubaker, and M. Bouhafs, A dynamical model for investigation of A3 point maximal spatial evolution during resistance spot welding using Boubaker polynomials, *Eur. Phys. J. Appl. Phys*., **44**, 317–322 (2008).
29. H. Labiadh, M. Dada, O. B. Awojoyogbe, K. B. Ben Mahmoud, and A. Bannour, *J. Differ Eq. Contin. Processes*, **1**, 51–66 (2008).
30. T. Ghrib, K. Boubaker, and M. Bouhafs, Investigation of thermal diffusivity — microhardness correlation extended to surface-intruded steel using Boubaker polynomials expansion, *Mod. Phys. Lett. B*, **22**, 2907–2915 (2008).

31. S. Lazzez, K. Boubaker, T. Ben Nasrallah, M. Mnari, R. Chtourou, M. Amlouk, and S. Belgacem, Structural and optoelectronic properties of InZnS sprayed layers, *Acta Phys. Pol. A*, **114**, 86–9880 (2008).
32. K. Boubaker and M. Bouhafs, Effects of combined radiative and convective heat transfer on temperature profile near plate surface heated by modulated source, *Int. J. Mod. Phys. B*, **21**, No. 11, 1903–1913 (2006).
33. M. De Otfried, *Semiconductors Data Handbook*, ISBN:3540404880, Birkhäuser (2003), pp. 338–339.
34. S. Picard, D. T. Burns, and P. Roger, Determination of the specific heat capacity of a graphite sample using absolute and diffusion methods, *Metrologia*, **44**, 294–302 (2007).
35. S. M. Stishov, A. E. Petrova, S. Khasanov, G. Kh. Panova, A. A. Shikov, J. C. Lashley, D. Wu, and T. A. Lograsso, Heat capacity and thermal expansion of the itinerant helimagnet MnSi, *J. Phys.: Condens. Matter*, **20**, 235222–235228 (2008).
36. M. V. Arx, O. Paul, and H. Baltes, Determination of the heat capacity of CMOS layers for optimal sensor design, *Sensors Actuators A*, **47**, Nos. 1–3, 428–431 (1994).
37. S. Dilhaire, S. Grauby, W. Claeys, and J.-C. Batsale, Thermal parameters identification of micrometric layers of microelectronic devices by thermoreflectance microscopy, *Microelectron. J.*, **35**, No. 10, 811–816 (2004).
38. K. Morimoto, A. Uematsu, S. Sawai, K. Hisano, and T. Yamamoto, Simultaneous measurement of specific heat capacity, thermal conductivity and thermal diffusivity of ferroelectric $Ba(Ti_{1-x},Sn_x)O_3$ ceramics by thermal radiation calorimetry, *Jpn. J. Appl. Phys.*, **41**, No. 11B, 6943–6953 (2002).
39. K. Morimoto, S. Sawai, and K.Hisanno, Specific heat capacity measurement at high temperature by thermal radiation calorimetry, in: *Proc. Int. Conf. on Microwave and Millimeter Wave Technology*, ICMMT'98 (1998), pp. 249–252.